Greenland Blocking Index daily series 1851-2015: analysis of changes in extremes and links with North Atlantic and UK climate variability and change

Short title: Greenland Blocking Index daily series 1851-2015

MS accepted 27 February 2018 by *International Journal of Climatology*

Edward Hanna[1], Richard J. Hall[1], Thomas E. Cropper[2], Thomas J. Ballinger[3], Leanne Wake[4], Thomas Mote[5], John Cappelen[6]

[1]School of Geography and Lincoln Centre for Water & Planetary Health, University of Lincoln, UK

[2]School of Earth and Ocean Sciences, Cardiff University, Wales, UK

[3]Department of Geography, Texas State University, USA

[4]Department of Geography and Environmental Sciences, Northumbria University, UK

[5]Department of Geography, University of Georgia, USA

[6]Danish Meteorological Institute, Copenhagen, Denmark

Corresponding Author: Edward Hanna, School of Geography, University of Lincoln, Think Tank, Ruston Way, Lincoln, LN6 7FL, UK, ehanna@lincoln.ac.uk

Abstract

We present a homogenised Greenland Blocking Index (GBI) daily record from 1851-2015, therefore significantly extending our previously published monthly/seasonal GBI analysis. This new time series is analysed for evidence of changes in extreme events, and we investigate the underlying thermodynamic and dynamic precursors. We compare occurrences and changes in extreme events between our GBI record and a recently published, temporally similar daily North Atlantic Oscillation (NAO) series, and use this comparison to test dynamic meteorology hypotheses relating negative NAO to Greenland Blocking. We also compare daily GBI changes and extreme events with long-running indices of England and Wales temperature and precipitation, to assess potential downstream effects of Greenland blocking on UK extreme weather events and climate change. In this extended analysis we show that there have been sustained periods of positive GBI during 1870-1900 and from the late 1990s to present. A clustering of extreme high GBI events since 2000 is not consistently reflected by a similar grouping of extreme low NAO events. Case studies of North Atlantic atmospheric circulation changes linked with extreme high and low daily GBI episodes are used to shed light on potential linkages between Greenland blocking and jet-stream changes. Particularly noteworthy is a clustering of extreme high GBI events during mid-October in four out of five years during 2002-2006, which we investigate from both cryospheric and dynamic meteorology perspectives. Supporting evidence suggests that these autumn extreme GBI episodes may have been influenced by regional sea-ice anomalies off west Greenland but were probably largely forced by increases in Rossby-wave train activity originating from the tropical Pacific. However, more generally our results indicate that high GBI winter anomalies are co-located with sea-ice anomalies, while there seems to be minimal influence of sea-ice anomalies on the recent significant increase in summer GBI.

Keywords: blocking, climate change, Greenland, jet stream, North Atlantic Oscillation, UK

1. Introduction

Greenland high-pressure blocking is a key measure of changes in North Atlantic and Northern Hemisphere atmospheric circulation and potential Arctic-mid latitude climate linkages (e.g. Woollings et al. 2008, Davini et al. 2012a, Hall et al. 2015, Hanna et al. 2015 & 2016, Mattingly et al. 2015, McLeod & Mote 2016, Overland et al. 2015 & 2016, Budikova et al. 2017, Ballinger et al. 2018a). Blocking is generally used to describe a large, quasi-stationary mid-latitude anticyclone that persists for at least a few days, and is associated with increased large-scale meridional flow (Rex 1950), but there is no clear consensus on an exact definition (e.g. Woollings et al. 2008). Greenland blocking events tend to be characterised by cyclonic upper-level Rossby wavebreaking, which distorts the climatological trough south of Greenland and if it persists for a few days transfers relatively warm subtropical air masses to high northern latitudes over Greenland (Woollings et al. 2008, Davini et al. 2012a, Hanna et al. 2016). Cyclonic wavebreaking also favours episodes of extreme poleward moisture transport along the west coast of Greenland (e.g. Liu and Barnes 2015). These events have been observed to co-occur with Greenland Ice Sheet (GrIS) melt episodes, including the extreme July 2012 melt event (e.g. Neff et al. 2014, Bonne et al. 2015). Since Greenland blocks typically lie well to the north of the jet stream they tend to divert rather than block the prevailing westerly airflow (DeWeaver & Nigam 2000, Luo et al. 2007a, Woollings et al. 2008, Davini et al. 2012a). The North Atlantic polar jet stream typically lies further south under blocked conditions (Hall et al. 2015), although bifurcated jet-steam conditions, with one branch going further north than normal over Greenland as in summer 2007, are also possible (e.g. Hanna et al. 2009, their Figs. 14 & 15).

Greenland blocking events last on average for ~6-9 days, develop from the retrogression of an unusually strong Atlantic ridge, and are sometimes preceded by European blocking (Davini et al. 2012a). McLeod & Mote (2015) linked the intensity of extreme Greenland blocking episodes since 1979 to precursor cyclones, which formed to the west of Greenland prior to the occurrence of peak blocking. Greenland blocking is heavily influenced by the underlying Greenland landmass and topography (with the mountainous ice sheet rising up to ~3 km above sea-level). The high north-south-oriented Greenland topography causes atmospheric ridging, and surface cooling by the ice sheet and adjacent snow cover can produce high air pressure near the surface, with anticyclonic curvature often observed in cirrus cloud features, making Greenland one of the sunniest regions for its latitude (Scorer 1988). As relatively cold dense air spills out from the surface as katabatic drainage (e.g. Orr et al. 2005), air sinks from higher levels to fill the void, which can cause heating and raised geopotential heights aloft.

Strong Greenland blocking episodes have been linked to exceptional surface melting of the GrIS (Hanna et al. 2014, Tedesco et al. 2016a), record wet weather in large parts of the UK in summers 2007 and 2012 (Overland et al. 2012, Hanna et al. 2016), and the highly unusual westward track of a major Hurricane (Sandy) which hit the US seaboard near New York in late October 2012 (Mattingly et al. 2015). Ballinger et al. (2018a) invoked increased Greenland blocking in autumn since 1979 to explain greater poleward transport of relatively warm air and reduced Baffin Bay sea-ice conditions, and coastal air temperature warming. Recent work also suggests an autumn/early winter Baffin Bay-Davis Strait-Labrador Sea (BDL) ice influence on the thermal high and Greenland blocking, which is not supported in spring/summer melt periods (Ballinger et al. 2018b). This involves surface warming over the BDL region, a weakening of prevailing westerly winds, and a pronounced westward movement of the Greenland block (Chen & Luo 2017). Greenland blocking, which can also be influenced by surface meteorological and glaciological changes over the ice sheet (Hanna et al. 2016), is therefore likely to have impacts on extreme weather and climate change over wide areas of the mid-latitude North Atlantic and areas well beyond Greenland.

Changes in Greenland blocking have recently been measured using the Greenland Blocking Index (GBI), which is defined using the mean 500 hPa (mid-tropospheric) geopotential height over the Greenland region of 60-80°N, 20-80°W (Fang 2004, Hanna et al. 2013, 2014, 2015 & 2016, Mattingly et al. 2015, McLeod & Mote 2015 & 2016) (Figure S1). Hanna et al. (2016) presented a long-running, homogenised monthly and seasonal GBI record based on a merging of the Twentieth Century Reanalysis Version 2c (hereafter 20CRv2c; Compo et al. 2011 & 2015) and NCEP/NCAR Reanalysis 1 (Kalnay et al. 1996), through post-processing that used splicing and breakpoint analysis. From their analysis, Hanna et al. (2016) found a significantly increasing GBI trend in summer in the last 1-3 decades that they ascribed to the Arctic amplification of global warming (Overland et al. 2016). Over this recent period, Hanna et al. (2016) also found that GBI had become significantly more variable from year to year in December: the cause of which remains uncertain but is related to a similarly more variable North Atlantic Oscillation (NAO) and Arctic Oscillation for the same calendar month (Hanna et al. 2015, Overland & Wang 2015). McLeod & Mote (2016) found an unusually high occurrence of extreme Greenland blocking episodes during 2007-2013, mainly in summer, compared with the rest of their 56-year record.

These previous studies are confined to analysing either daily or monthly and seasonal GBI changes since 1948. It is important to extend these observational analyses of recent Greenland blocking changes, given current uncertainty in the representation by climate models of North Atlantic jet-stream and blocking changes and potential Arctic climate-mid latitude weather linkages (Hall et al. 2015, Barnes & Screen 2015, Overland et al. 2016, Hanna et al. 2017).

Here we extend the work of Hanna et al. (2016) to present a fully homogenised daily GBI record from 1851-2015, relate extreme daily GBI events to atmospheric circulation and surface heating anomalies, and analyse our new record for evidence of any significant changes in the frequency of daily GBI episodes that may be related to climate change and have potential interactions with – and impacts on – mid-latitude North Atlantic circulation conditions south of and downstream of Greenland, including over the UK region. We examine the relationship between daily GBI and NAO over the seasonal cycle, compare relative changes in extreme daily GBI and NAO events within the last 165 years, and relate extreme daily GBI events to anomalous UK seasonal weather. We use our new, long homogenised daily GBI series together with a recently-published long NAO daily series to test the following dynamic meteorology hypotheses. These include the proposal by Woollings et al. (2008) that negative NAO is simply a high frequency of Greenland blocking events, and a positive NAO is the lack of such an event. Alternatively, Barriopedro et al. (2008) suggested that NAO changes may drive North Atlantic blocking trends. A further interpretation by Luo et al. (2007b) suggests that, since on the weekly timescale Greenland blocking and the negative phase of NAO events have the same spatial structure and lifetime characteristics, negative NAO events are identical to Greenland blocking episodes rather than arising from or driving the latter. Finally we also consider how the recent marked autumn/winter sea-ice decline west of Greenland, and the state of the North Pacific atmospheric jet further upstream, may affect Greenland blocking and the North Atlantic jet.

Section 2 describes the datasets and statistical analysis methods used in this study, Section 3 summarises the results, which are presented by monthly/seasonal and then extreme daily GBI analyses in turn; a discussion and summary of the results is provided in Section 4.

2. Datasets and methods

Greenland Blocking Index (GBI) daily data for 1948-2015 were calculated based on NCEP/NCAR reanalysis 500 hPa geopotential height data downloaded for a grid of 35 well distributed points (Figure S1), which were then averaged to produce daily values for the standard GBI region of 60-80°N, 20-80°W. Older daily GBI data for 1851-1947 were derived from the 20CRv2c (Compo et al. 2015), but needed homogeneity adjustments and splicing against the NCEP/NCAR-based GBI record for the common overlap period. The same homogenisation and splicing methods and coefficients used for the monthly series (Hanna et al. 2016) are applied to the daily series.

We adjusted the NCEP/NCAR daily GBI values because the National Oceanographic & Atmospheric Administration Earth Systems Research Laboratory Physical Sciences Division (NOAA ESRL PSD) online web tool at https://www.esrl.noaa.gov/psd/data/timeseries/daily/ only allows daily data to be downloaded for points rather than areas. We acquired data for every 5° latitude and 10° longitude over the GBI region (35 points in total) but this gives an area-weighting towards high northern latitudes (denser coverage of points) that needs correcting. This was done using regression splicing of monthly means of the 35-point daily time series against the full area-averaged, area-weighted monthly time series downloaded separately, with excellent agreement between the adjusted daily NCEP/NCAR GBI series and the original monthly NCEP/NCAR GBI series.

Each GBI daily value was then normalised with respect to the mean and standard deviation of all the daily GBI values for 1951-2000 for that day of year. This procedure provides the advantage of avoiding occasional jumps between months that would otherwise have arisen from the use of monthly coefficients derived in our previous analysis. Monthly means of daily 20CRv2c and NCEP/NCAR GBI agree extremely well (r=0.92-0.99) for the 1948-2014 overlap period. Daily data are an extension of monthly GBI time series presented in Hanna et al. (2016).

McLeod & Mote (2016) define an extreme GBI event as having at least 5 consecutive days where the GBI attained at least the 97^{th} percentile of all 1958-2013 daily GBI values for a 7-day window centred on that date. However, unlike McLeod & Mote (2016), we do not pre-process the data using a low-pass filter, as we prefer to preserve the high-frequency GBI signal. We instead take extreme daily GBI events as being above or below certain thresholds (e.g. 2 or 3 standard deviations (σ) above or below the respective long-term mean for that day of year), and analyse changes in the frequency of these events with time. We focus initially on GBI events exceeding 3σ for at least three consecutive days, as they are statistical outliers and represent a manageable number of extreme events.

We also co-analyse extreme GBI episodes in comparison with changes in extreme daily NAO events, based on a temporally comparable Azores-Iceland station-based NAO dataset (Cropper et al. 2015, hereafter abbreviated C15), supplemented with the Climate Prediction Centre (CPC)'s principal component-based daily NAO index for the period since 1950 (Barnston & Livezey 1987; http://www.cpc.ncep.noaa.gov/products/precip/CWlink/pna/nao.shtml), and with North Atlantic polar jet stream daily speed and position (Hall et al. 2015; Hall, 2016). Jet speed and position are calculated using the method of Woollings et al. (2010) applied to 20CRv2c data. Mean daily zonal wind speeds over the North Atlantic (0-60W,16-76N) are averaged over 900-700 hPa. A zonal mean wind speed is then calculated for each 2º latitude band, and these zonal means are low-pass filtered using a 61-point Lanczos filter to remove synoptic scale (<10 days) variability (Duchon, 1979). The latitude band with the maximum mean zonal wind speed for each day is taken as the jet latitude, and the zonal mean wind speed at that latitude is the jet speed. Monthly and seasonal averages are calculated for each jet metric.

To test the hypothesis of Woollings et al. (2008) outlined above, we first compare the numbers of days per month above or below various GBI values with monthly mean NAO values and with the numbers of days per month that have NAO values of similar magnitude but opposite sign (i.e. the numbers of GBI>2 days are compared with numbers of NAO<-2 days for each month and season). We also compare the numbers of moderate (<-1 & >1σ) and extreme (<-2 & >2σ) NAO days with monthly mean GBI values. Second, we determine any leads and lags between respective changes in GBI, NAO and North Atlantic jet stream metrics in the extreme GBI event daily case studies mentioned above. To help elucidate NAO-GBI interactions we investigate seasonal composites of 500 hPa geopotential height anomalies over Greenland for daily NAOI negative values below stepped NAOI thresholds [i.e. a composite (mean) of days with NAO values where -1.5σ < -1σ, then further composites with progressively more extreme z-values in -0.5σ steps], based on 20CRv2c data spanning 1850-2014.

We additionally use 20CRv2c composite plots of 500 hPa geopotential height and vector winds, alongside 850 hPa temperature anomalies for seasons and months having the highest numbers of moderately high GBI (GBI>1) days. Since these plots are based on 1851-2014, they represent nearly the full period of GBI record. Hadley Centre Sea Ice and Sea Surface Temperature (HadISST) sea-surface temperature (Rayner et al. 2003) and HadISST2.2 sea-ice data (Titchner & Rayner 2014) are used to elucidate GBI-sea ice relationships on the regional basis around Greenland.

Finally we compare our GBI daily series with daily time series of both Central England Temperature (CET; Parker et al. 1992) and England & Wales Precipitation (EWP; Alexander & Jones 2001), where these long-running and well-documented meteorological records allow us to track the potential impact of GBI changes for most of the period of record on North Atlantic polar jet-stream conditions over the UK, i.e. downstream of Greenland.

Pearson's product-moment correlation, bivariate linear regression and composite analyses are the main statistical methods used here. Statistical significance of calculated trends is tested using an online t-test calculator http://www.graphpad.com/quickcalcs/pvalue1.cfm based on Abramowitz & Stegun (1965). Statistical significance is defined using a standard $p \leq 0.05$ threshold. Datasets are de-trended prior to carrying out correlation.

The analysis covers all months but – because of a mass of data – focuses on key summer and winter months (June, July and December) for which intriguing changes in

North Atlantic atmospheric circulation have recently been identified, especially for the period of rapid Arctic sea-ice decline since 2007 (Serreze & Stroeve 2015); these changes include a more meridional jet-stream flow in early summer and increased variability in circulation metrics during December (Overland et al. 2012; Hanna et al. 2015 & 2016; Overland & Wang 2015). Standard 3-month meteorological seasons are used (DJF, MAM, JJA, SON). Throughout the paper, where seasonal data/analysis are discussed, winter (DJF) seasons are denoted by the year of the January.

3. Results

3.1 Monthly and seasonal GBI analysis

3.1.1 Long-term/secular changes in GBI and NAO

Cumulative annual and monthly totals of daily GBI are shown in Figure 1. The annual data show upward inflections in the cumulative GBI curve from ~1870-1900 and ~2000-2015, and a decline during 1970-1990. These features are also apparent in the cumulative time series for the summer months but are largely absent in winter. The recent (post-2000) accumulation of high GBI daily values is particularly strong for August relative to June and July. September also shows a similarly striking recent increase to the summer months, while October and November do not. This therefore reflects an inter-seasonal summer progression of this interannual change. There is less secular change in other seasons compared with summer, although January and April show marked long-term declines in GBI.

Mean numbers of GBI days for different thresholds (GBI>0,1,2; NAO<0,-1,-2) for each calendar month, year and summer and winter seasons are summarised in Tables 1, S1 & S2. These show clusterings of high numbers of GBI days for summer and the year as a whole for the last decade (2006-2015) relative to the climatological mean. For example the number of summer days with GBI values >0 (>1) is 69.5 (35.6) relative to (1981-2010) climatological means of 47.7 (18.6) [Table S1(a) & Table 1]. The difference is even more striking for number of summer days having GBI>2 (10.0 relative to 3.8) (Table S1b). However, other months do not have record numbers of positive /high-value GBI days at the end of the period: for example, January, December and winter (May and September) generally have record numbers of such days during the 1960s (1950s and 1930s respectively), while October and November generally have their greatest numbers of positive GBI days during the second half of the Nineteenth Century (Tables 1 & S1a). In contrast, Table S2 showing changes in numbers of station-based NAO days, does not show any recent (post-2000) record clusterings of negative/low-value NAO days, except (marginally) for December 2000-2009 for NAO<-1,-2. This may be related to the use of a station-based NAO index in summer since the PC-based NAO index does show recent clusterings of low NAO index days in summer (Table S3). However, there is a pattern where certain months with high numbers of positive GBI days for particular decades show correspondingly high numbers of negative NAO days for the same months/decades (e.g. January and winter for the 1960s; March, 1950s).

A visualisation of changes in numbers of annual and summer and winter seasonal GBI and NAO days is shown in Figures 2 and S2. These graphs show little change in numbers of GBI>0 days, but clear upward trends in numbers of more extreme

GBI>1,2 days, for the period as a whole (Figure 2a-c). However, overall trends are significant only in 3/6 cases: for summer for moderately high GBI>1 episodes, and for winter and annual for more extreme GBI>2 events. The 2010 record peak in annual GBI>2 days is only slightly above previous similar peaks in 1878 and 1887, while 2008 and 2011 peaks in summer GBI>2 days are preceded by several similar peaks during the early Twentieth Century. Regarding the number of GBI>1 days, there are recent exceptional peaks in all three series: 2010 (annual and winter) and 2012 (summer). By contrast, Figure S2 shows few cases and insignificant trends in negative NAO days, and that peaks in such events in the last decade are unexceptional in the context of the overall NAO record.

These results are supported by the trend analysis for summer and winter and selected months presented in Table 2, which clearly shows many significantly positive GBI trends for the recent 1990-2015 period but relatively few trends for longer/earlier and intermediate periods (Table 2a). Within the last 26 years, significant upward trends in numbers of GBI days>0,1 are almost ubiquitous for summer and annual series but are less consistent for winter data. Also of note is a significant increase in the annual number of days with GBI>1 since 1900. There were few sustained changes in the monthly or seasonal standard deviation of daily GBI values during the period of record. A similar analysis of trends in numbers of days with negative NAO values (Table S4) indicates no significant trends after 1990, corroborating the earlier results from Tables 1, S1 and S2: i.e. recent increasingly common high GBI days (which are primarily a summer phenomenon) have not been generally mirrored by more frequent low NAO days. Again, this apparent breakdown in the relation between high GBI and low NAO is likely to be linked to our primary use of a station-based NAO series rather than necessarily indicating a real breakdown in the GBI-NAO relation.

Next we examine rank-ordered numbers of high GBI (GBI>1) days for selected summer and winter seasons (Table 3). Two recent years 2012 and 2010 stand out as having exceptionally high numbers of positive GBI days in summer and winter respectively, in accordance with previous work finding record high values in these years based on seasonal GBI data (Hanna et al. 2016). However, it is also clear from this table that, despite there being some relation, there is not always a clear correspondence between the numbers of high GBI and low NAO days for particular months and years. For example, June had the greatest number of GBI>2 days in 1891 and 1897 but the greatest number of NAO<-2 days was in 1903. Also, 1911, which had some of the greatest numbers of NAO<-1,-2 days in summer, had a smaller number of positive GBI values than several other summers.

3.1.2 GBI relation with NAO

Figure 3 summarises correlations between daily GBI and NAO values for the full (1851-2015) period, including variations in mean daily correlations over the seasonal cycle (i.e. correlation calculated for 1 January for all years, then repeated for each day of year; Figure 1a,b) and interannually (correlation calculated for 1851 for all days, then repeated for all years; Figure 1c). These generally indicate the strongest correlations during winter and spring, and weakest correlations (although all still significant) in summer. GBI-NAO correlations are typically ~-0.6 but range from ~-0.4 in mid-summer to ~-0.7 in late winter and early spring. Figure 3(b) is similar to Figure 3(a) but includes both station-based and principal-component based (CPC) NAO indices for the 1950-2015 common period. Inter-seasonal correlations hold up well, and actually increase slightly in summer, when the CPC NAO series is used. This indicates that the summer drop-off in seasonal correlations is due to use of a station-based NAO index that does not fully capture migration of the NAO centres of action (i.e. the regions of maximum surface pressure change) rather than a real physical weakening of the GBI-NAO relation. Regarding long-term changes, Figure 3(c) shows that correlations are notably lower for the pre-1880 period, which may reflect limitations with these early parts of the GBI and NAO series, and especially in the realistic representation of mid-tropospheric geopotential height variations over Greenland at the daily timescale. For example, 20CRv2c globally-averaged geopotential fields before about 1865 appear to be biased low by errors in marine pressure observations that were assimilated by the reanalysis (https://www.esrl.noaa.gov/psd/data/gridded/20thC_ReanV2c/opportunities.html). Alternatively, gridded sea-level-pressure fields were used instead of meteorological station data as a basis for constructing the C15 daily NAO series from the 1850s to the early 1870s, with the latter time marking a jump in the running correlations.

Monthly and seasonal correlation coefficients between numbers of days per month or season above or below specified GBI thresholds and (a) monthly or seasonal mean GBI, (b) monthly or seasonal mean NAO and (c) numbers of days per month or season above and below NAO thresholds of opposite sign and magnitude are shown in Table 4. Subset (a) shows very strong ($r \geq 0.90$) correlations between mean GBI and numbers of positive GBI days (GBI>0) for all months and seasons listed. The correspondence is almost as strong for numbers of GBI>1 days (0.88 for annual) and still 0.72 (-0.77) for numbers of GBI >2 (<-1) days but is much less strong at -0.48 (annual) for GBI<-2 days. There is also generally good agreement between numbers of thresholded GBI days and monthly or seasonal mean NAO, which is strongest for GBI>1 values (e.g. -0.81 for winter and -0.44 for summer), and almost as strong for GBI>2 values. The correspondence is a lot less strong for thresholded negative GBI values, falling to r = 0.21 (0.06) for winter (summer) based on the GBI<-2 value subset. Correlations of numbers of GBI days above or below given thresholds with monthly mean NAO are consistently weaker for summer relative to winter (Table 4b). Table 4(c) indicates generally good correspondence between numbers of high (low) GBI and low (high) NAO events (e.g. r = 0.64 for annual data). However, following the above pattern, there is less agreement between numbers of extreme negative GBI (GBI<-2) days and numbers of extreme positive NAO (NAO>2) days (r = 0.23). Table 4(d) confirms the above pattern by showing a stronger (less strong) association between numbers of extreme negative (positive) NAO days and monthly or seasonal mean GBI values.

Our stepped threshold analysis of geopotential height anomalies and patterns for successively more negative NAO1 conditions shows high GPH500 clearly linked with Greenland blocking, i.e. the anomalies are centred over Greenland, in winter (Figure S3). In summer the highest GPH500 anomalies are offset to be centred between Greenland and Iceland, and are centred near Iceland for the lowest NAO cases ($<-3.5\sigma$). The weaker summer GPH500 anomalies and the eastward shift in the NAO pattern are likely to be responsible for the NAO-GBI relation in summer being generally less strong than in winter (Table 4). Winter low NAO (high GBI) cases are associated with low

GPH500 anomalies across much of central Europe, parts of Scandinavia and Russia but this is not the case for summer (Figure S3).

3.1.3 GBI relation with Northern Hemisphere mid-high latitude circulation and sea-ice anomalies

Composite plots showing anomalies of 500 hPa geopotential height (GPH500), vector winds, 850 hPa temperatures (T850), and sea-ice-concentration (SIC) for the five seasons/years with the highest numbers of GBI>1 days (years listed in Table 3), are shown in Figure 4. For summer (JJA) (Figure 4b), these show a GPH500 anomaly aligned SSW-NNE with a main focus ~70 m centred just off the southwest Greenland coast. Meanwhile, modest negative GPH500 anomalies of ~-20 m are located over Ireland and in the Atlantic just west of the UK. Low heights are also evident over western and northern Alaska and the Bering Strait. The corresponding composite vector wind anomaly plot shows a southward-displaced North Atlantic jet, with its core extending eastwards south of the UK, with stronger-than-normal westerlies over Biscay and north-east anomalies over much of the mid northern North Atlantic around Iceland and south of Greenland (Figure 4d). Warm air anomalies are located over west Greenland, the Labrador Sea and Canadian Archipelago, with a striking 3°C warm spot over extreme north Siberia near the coast (Figure 4f). This may reflect increased seasonal sea-ice depletion in these high GBI years, as the wind-vector anomaly plot shows an offshore (southerly) wind bias (Figure 4d). This is supported by SIC anomalies which are biased low in the same region during conditions of high GBI in summer (Figure 4h). However, pockets of moderate SIC anomalies in coastal areas of Greenland and Baffin Bay suggest a minimal contribution of localised open-water anomalies to +GBI anomalies, although sea-surface temperatures (SSTs) are biased warm south of Greenland (Figure 4j). Advection of relatively cold Arctic air over the Bering Strait region may be responsible for the low GPH500 and T850 anomalies centred over Alaska, and this is also linked to cold SSTs in that region (Figures 4b,d,f,j).

Seasonal anomalies for the five winters with the greatest number of GBI>1 days (Table 3b) are now examined (Figure 4a,c,e,g,i). In comparison with summer, the top five winters show a much greater (about double the magnitude) and more zonally-aligned GPH500 anomaly, which extends further west over the Labrador Sea and Canadian Archipelago (Figure 4a). The high GPH500 anomaly extends towards Svalbard and over central Russia, rather than across the central Arctic Ocean as in summer, and there is a much wider swath of negative GPH500 heights and low pressure extending west-east entirely across the mid-Atlantic and into northern Europe, which is most intense over northern France and south-western parts of the UK. Anomalous southerly airflow extends north over the Canadian Arctic Archipelago, Labrador Sea and over west Greenland (Figure 4c). The corresponding T850 plot shows an intense warm spot centred over the Labrador Sea and Baffin Bay areas, and cold anomalies focused over Siberia, Scandinavia and much of eastern, central and northern-western US (Figure 4e). In contrast with the summer situation around Greenland, the SIC anomaly pattern in winter over parts of southern Baffin Bay, Davis Strait and the northern Labrador Sea (Figure 4g) appears co-located with the GPH500 anomaly shown in Figure 4a. The upper-level anticyclone is centred over a marginal ice zone characterised by anomalously low ice coverage, allowing upward heat fluxes from the open ocean or young sea ice to sustain the ridge aloft. The enhanced near-surface warming weakens prevailing westerly winds via the thermal-wind principle and prolongs pre-existing Greenland blockings (Chen & Luo 2017). SST anomalies are generally high around south and west Greenland but are low immediately off the east and south-east coasts (Figure 4i).

3.2 Extreme GBI events on daily timescale – North Atlantic synoptic characteristics and precursors

GBI episodes of ≥3(≤-2.5)σ where these thresholds were attained or surpassed for at least three consecutive calendar days are summarised in Table 5. These events are concentrated in certain parts of the record: for example, with 1875-1900 and 2002-2010 accounting for respectively 10 and 12 out of 32 anomalously high GBI events in Table 5(a); these peak periods are in accordance with our cumulative daily GBI results reported in Section 3.1.1. Of particular note is a clustering of unusually high GBI episodes during mid-October in several successive years: 2002, 2003, 2005 and 2006 (2004 October with three consecutive days having GBI values ≥2.85, with the last two of these days GBI>3, fell only slightly under the threshold). Is this unprecedented sequence of extreme GBI events just a statistical quirk or does it reflect a seasonally-sensitive physical forcing mechanism that has perhaps been triggered or exacerbated by Greenland climate change and sea-ice loss in the wider Arctic region?

To help set these extreme GBI episodes (Table 5) in a broader context and discern possible precursors and impacts, we analyse atmospheric circulation conditions and anomalies over the wider North Atlantic region and their evolution at the daily timescale for a period from 5 days before to 5 days after these episodes (Figure 5).

Mean synoptic conditions during the 2002, 2003, 2005 and 2006 October episodes indicate that the North Atlantic jet stream moved south by ~7° latitude and first decreased its speed by ~25% during the five days prior to the highest part of these October GBI phases but subsequently accelerated to above initial values during the time of peak GBI; although the C15 station-based Azores-Iceland NAO index showed an inverse but similar symmetric response to GBI, the principal-component-based CPC NAO index minimum is time-lagged by 2 or 3 days with respect to the peak in the GBI cycle (Figure 5a). There is a similar clustering of high GBI events in late September and October during the late Nineteenth and early Twentieth Centuries [1880 (x2), 1888, 1895 and 1916; Table 5a], and a further graph shows the synoptic evolution of these earlier events (Figure 5b). The southward movement of the jet 3-5 days before the rise in Greenland blocking is evident but in this case there is little systematic change in jet speed, while – similar to the above - there does not seem to be any lag between the GBI maximum and the Azores-Iceland NAO minimum (there are no available CPC NAO data before 1950 for comparison purposes). A composite graph of high GBI episodes during summer (Figure 5c) shows the jet jumping south, with the main shift 2-3 days before peak GBI, but not much change in jet speed (a slight slowdown, then speed-up, of <10%). CPC NAO changes almost mirror the GBI changes, while the Azores-Iceland NAO reaches its minimum 4 days following peak GBI. The winter extreme high GBI composite (Figure 5d) shows the jet jumping south >10° 1 day before peak GBI but with little change in speed, while both NAO records approximately (inversely) mirror the GBI changes.

Turning our attention now to a notable clustering of extreme *low*/negative GBI events which occurred in the springs of 1897, 1906, 1934, 1990, 1993, 2011 and

2013 (Table 5b), the North Atlantic jet shifts north on average by ~9° while simultaneously strengthening from ~12 to 16 m s^{-1} from 3 days ahead of GBI minimum. The Azores-Iceland (CPC) NAO positively peaks ~1 (2-5) days after the lowest negative GBI value (Figure 5e). Again, the jet typically shifts before the GBI reaches its most negative value, with the accompanying change in the NAO index tending to lag slightly behind.

3.3 Comparison of GBI and NAO daily series with UK climate indices

Daily GBI and C15 Azores-Iceland NAO series are correlated with CET and EWP UK climate indices for both the seasonal cycle and interannually for the full periods of overlapping records (1851-2015 for CET and 1931-2015 for EWP), in the same way as described for Figure 3 in Section 3.1.2, and the results are presented in Figure 6. Relatively weak correlations for CET range from ~±0.4 in winter to near zero in summer, with correlations generally being of opposite sign for GBI and NAO (Figure 6a). For the seasonal plots correlations greater than ±0.15 are significant, so there is a fairly persistent positive (negative) association between CET and NAO (GBI) between November and April but correlations are insignificant for the rest of the year; also, annual mean correlations have been relatively stable for the last century and a half (Figure 6b). Winter 2009/10, which had a record high number of positive GBI days in the whole 165 years of record (Table 3b), was characterised by unusually cold, snowy winter weather over the UK (e.g. Hanna et al. 2017); the following winter 2010/11 also featured severe cold over the UK, including the coldest December CET since 1890, and has the fourth greatest number of highly positive winter GBI days. For EWP, correlations with NAO and GBI are overall weaker but are again of opposite sign and are briefly and significantly positive for NAO in December and approach the significance threshold (positive) for GBI in summer; as for CET, there is no sign of a systematic shift of these correlations over time (Figure 6b,d). However, in summer CET/EWP correlations will be low with station-based NAO as the latter does not capture shifts in centres of action of the summer NAO regime (i.e. there is a significant seasonal shift in the locations of maximum surface pressure variation). Extreme positive GBI events tend to be associated with both relatively low CET and with moderate to high (>2 mm day^{-1}) EWP; conversely, extreme negative GBI episodes typically coincide with near- or above-average CET and generally lower EWP, with several notably high CET events in spring and summer values (Table 5). Notably, referring to the clearly record high numbers of positive GBI days in summer 2012 (Table 3a), this was a record-breaking wet summer in England and Wales – the wettest for a century – and was also cooler than average (Parry et al. 2013; Hanna et al. 2017).

4. Discussion/summary

We have compiled, presented and analysed a new homogenised daily GBI dataset from 1851-2015. This valuable extension enabled an analysis of high-time-frequency (daily) weather events, and their changing frequency/intensity in the context of changing climate. Long-term monthly and seasonal statistics have also been computed, reinforcing findings from a previous study (Hanna et al. 2016). Recent increases in the frequency of extreme high GBI events are noted for June, July and August (Table 1) but are not always mirrored by increases in low NAO episodes (Table S2b), although results are sensitive to the type of NAO index used (Table S3b). Steep increases in cumulative daily GBI for 1870-1900 and 2000-2015 are noted for the overall annual time series and summer monthly series but are much more muted for winter monthly series (Figure 1). These GBI trends are broadly in line with our previous results based on monthly/seasonal GBI analysis (Hanna et al. 2016). The summer increase in cumulative daily GBI is much more marked for high summer (Figure 1), and this may result from cumulative positive feedbacks acting more strongly in August, relative to June and July, during progressively warmer Greenland summers since 2000 (Hanna et al. 2008, 2012, 2014; Tedesco et al. 2016b).

The comparisons between monthly counts of the number of thresholded GBI days and both the monthly mean NAO and numbers of thresholded NAO days are generally stronger for positive GBI and negative NAO (Table 4). Also there is a slight lag (mean ~1 day) between peak GBI and record NAO over a number of extreme daily events, although both the extreme GBI and NAO values tend to be preceded by a southward (northward) movement of the jet under positive (negative) GBI (Figure 5 & Table 5). Our findings generally support the Woollings et al. (2008) hypothesis that negative NAO arises from Greenland blocking and that positive NAO mainly represents the absence of blocking (rather than ‘anti-blocking’ or negative GBI conditions). This is also in agreement with the results of Davini et al. (2012b), who found that the first Empirical Othogonal Function of the 500 hPa geopotential height over Europe and the North Atlantic did not resemble the NAO for GBI- cases but more closely resembled an East-Atlantic circulation pattern (e.g. Hall et al. 2015; Hall & Hanna 2018) and that North Atlantic jet variability was then no longer related to Greenland blocking changes. Also in support of our findings that high-GBI and low-NAO events do not always align, Rimbu et al. (2017) found that stable-isotope variations in GrIS cores are more closely related to measures of Atlantic-European/Greenland blocking than the NAO index.

Our composite analysis of seasonally high GBI events (Figure 4) indicates a strong winter GBI signal linked to positive sea-surface temperature anomalies and negative sea-ice anomalies/freeze delays persisting into autumn. This relationship does not necessarily hold in spring when SSTs are relatively lower around the marginal ice zone west of Greenland as proximate air-sea fluxes tend to be negative (toward the surface) (Fenty & Heimbach 2013) including around the time of unseasonably early melt onset (Ballinger et al. 2018b). The winter co-location of high 500 GPH anomaly with low sea-ice anomalies suggests possible forcing in the form of ocean-atmosphere heat release through leads or new, thin ice cover, following the mechanism proposed in Ballinger et al. (2018a). Conversely, we have shown a likely minimal contribution of sea-ice anomalies to positive GBI anomalies in summer, while the relatively low summer air-sea temperature difference suggests a much more muted effect of SST anomalies around southern Greenland. On the basis of these results, we suggest that different mechanisms - relatively greater ocean-atmosphere heating in autumn - may enhance, or help sustain, blocking at these different times of year although this warrants further investigation.

Regarding the mid-2000s (2003-2006) clustering of extreme high GBI events in mid-October, we hypothesize that this may be related to the recent rapid loss of sea-ice to the west of Greenland, as the latest Baffin freeze dates since 1979 (i.e. 1 sigma events) have all occurred since 2002 (ranked 3rd latest) with 2006 marking the latest, and 2003 and 2005 freeze onset was later than normal (≥+0.5 sigma) (Markus et al. 2009; Ballinger et al. 2018a). Three out of four of these years had reduced sea ice in the northern part of Baffin Bay compared with 1979-2016 (ERA-I) climatology, although the pattern in 2005 was somewhat different, with a positive ice anomaly in much of the region (Figure S4). However, as these SIC anomalies are in confined areas typically characterised by low/thin ice coverage (climatological SIC=0.1-0.4), it is uncertain to what extent they may be responsible for such anomalous GBI values. Also, other years around that period, for example 2007 (Figure S4), have similar SIC anomalies but are not associated with anomalously high GBI. Nevertheless, we posit an autumn open-water linkage (south Baffin Bay, Davis Strait, north Labrador Sea) to extreme positive GBI, with possible upward heat contribution for north Baffin Bay in thinner-than-average years such as 2005.

Benedict et al. (2004) suggest that cyclonic (anticyclonic) wavebreaking displays a NW-SE (NE-SW) tilt. Under high GBI conditions, therefore, this tilt tends to deflect cyclones south (Priestly et al. 2017), which naturally gives rise to more negative NAO conditions, which over much of the UK are typically relatively cold and dry in winter but wet in summer (Hall & Hanna 2018). Rossby wave breaking in the east Atlantic is noted to precede the main/peak change in the jet stream in that region by ~2 days, and this is in accordance with our finding that the NAO low point sometimes lags peak GBI by 1-2 days. Benedict et al. (2004) also suggest that the remnants of the wavebreaking, which originates from transient eddies from far upstream, form and maintain the NAO; when wavebreaking stops, the NAO phase decays. Therefore the GBI may be remotely forced, or at least influenced, from as far afield as the Pacific, rather than simply locally formed. This might be especially important for the negative NAO (positive GBI) phase, as suggested by Ding et al. (2014) and Trenberth et al. (2014). According to their hypothesis, a Rossby-wave train could act to transmit SST signals from the central Pacific to Greenland and north-east Canada, and the high GBI events are primarily an adiabatic response to concomitant changes in the upper-troposphere circulation. Moreover there is mounting evidence that - in advecting energy and moisture polewards - such planetary wave trains may influence Arctic sea-ice cover (Yoo et al. 2012, Park et al. 2015, Baggett & Lee 2017, Ding et al. 2017) and therefore Greenland blocking.

This concept of tropical Pacific forcing of Greenland blocking is supported by evidence of equatorward perturbations of the North Pacific jet prior to the extreme high October (2002-2006) GBI episodes (Figure S5), consistent with Franzke et al. (2004). In addition, three of the four extreme October positive GBI events (2002, 2005 & 2006) were preceded by anomalous high pressure over Scandinavia, which is consistent with anomalous European blocking sometimes being a precursor of Greenland blocking (Davini et al., 2012a, McLeod and Mote, 2015). While a sample of four events is far from conclusive, these upstream and downstream dynamical associations suggest that the coincident extreme GBI events in October are unlikely to be more solely forced by local sea-ice anomalies. Conversely, a less consistent picture is evident for the negative GBI events in spring.

Whatever the dominant mechanism(s) of the recent record (e.g. October, mid-2000s) GBI events and long-term positive summer GBI trend, we anticipate that our new daily GBI record will be useful for various further meteorological/climatological and glaciological studies of the recently observed rapid changes on the Greenland Ice Sheet, and will help to set recent extreme events (e.g. the extreme melts of 2012 and 2015) in a longer-term climatic context, as well as helping to unravel new aspects of atmospheric forcing mechanisms of Greenland change. It will also be important to examine the fidelity of Greenland blocking in climate-model projections (e.g. CMIP5/6), so that they can better represent past, present and future Greenland Blocking (and associated NAO) changes. Greenland blocking is intrinsically connected to GrIS mass balance (Hanna et al. 2013, 2014, Hofer et al. 2017, van den Broeke et al. 2017) and, by extension, global sea-level changes. Greenland blocks are importantly associated with meteorological/climatological effects and impacts downstream and further south (e.g. over Northwest Europe). Fully homogenised, updated daily GBI time series will be made available (on publication) from: http://staff.lincoln.ac.uk/ehanna

Acknowledgements

We thank the Met Office for provision of CET and EWP data. We acknowledge the NOAA ESRL PSD for the provision of NCEP/NCAR and 20CRV2c reanalysis data, and the CPC for NAO data. Support for the Twentieth Century Reanalysis Project dataset is provided by the U.S. Department of Energy, Office of Science Innovative and Novel Computational Impact on Theory and Experiment program, and Office of Biological and Environmental Research, and by the National Oceanic and Atmospheric Administration Climate Program Office. We thank three anonymous reviewers whose comments helped improve the manuscript.

References

Abramowitz, M., I.A. Stegun (1965) *Handbook of Mathematical Functions: with Formulas, Graphs, and Mathematical Tables.* Dover Books on Mathematics.

Alexander, L.V., P.D. Jones (2001) Updated precipitation series for the U.K. and discussion of recent extremes. *Atmos. Sci. Lett.*, doi:10.1006/asle.2001.0025.

Baggett, C., S. Lee (2017) An identification of the mechanisms that lead to Arctic warming during planetary-scale and synoptic-scale wave life cycles. *J. Atmos. Sci.* 74, 1859-1877.

Ballinger, T.J., E. Hanna, R.J. Hall, J. Miller, M.H. Ribergaard, J.L. Høyer (2018a) Greenland coastal air temperatures linked to Baffin Bay and Greenland Sea ice conditions during autumn through regional blocking patterns. *Clim. Dyn.*, 50, 83-100.

Ballinger, T.J., E. Hanna, R.J. Hall, T.E. Cropper, J. Miller, M.H. Ribergaard, J.E. Overland, J.L. Høyer (2018b) Anomalous blocking over Greenland preceded the 2013 extreme early melt of local sea ice. *Ann. Glaciol.*, in press.

Barnes, E.A., J. Screen (2015) The impact of Arctic warming on the midlatitude jetstream: Can it? Has it? Will it? *WIREs Clim. Change* 6, doi: 10.1002/wcc.337.

Barnston, A.G., R.E. Livezey (1987) Classification, seasonality and persistence of low-frequency atmospheric circulation patterns. *Mon. Wea. Rev.* 115, 1083-1126.

Barriopedro, D., R. García-Herrera, A.R. Lupo, E. Hernández (2008) A climatology of Northern Hemisphere blocking. *J. Clim.* 19, 1042-1063.

Benedict, J.J., S. Lee, S.B. Feldstein (2004) Synoptic view of the North Atlantic Oscillation. *J. Atmos. Sci.* 61, 121-144.

Bonne, J.-L., H.C. Steen-Larsen, C. Risi, M. Werner, H. Sodemann, J.-L. Lacour, X. Fettweis, G. Cesana, M. Delmotte, O. Cattani, P. Vellelonga, H.A. Kjaer, C. Clerbaux, A.E. Sveinbjörnsdóttir, V. Masson-Delmotte (2015) The summer 2012 Greenland heat wave: In situ and remote sensing observations of water vapor isotopic composition during an atmospheric river event. *J. Geophys. Res. Atmos.* 120, 2970-2989.

Budikova, D., T.W. Ford, T.J. Ballinger (2017) Connections between north-central United States summer hydroclimatology and Arctic sea ice variability. *Int. J. Climat.* 367, 4434-4450.

Chen, X., and D. Luo (2017) Arctic sea ice decline and continental cold anomalies: Upstream and downstream effects of Greenland blocking. *Geophys. Res. Lett.* 44, 3411–3419.

Compo, G.P. et al. (2011) The Twentieth Century Reanalysis project. *Q.J.R. Meteorol. Soc.* 137, 1-28.

Compo, G.P. et al. (2015) NOAA/CIRES Twentieth Century Global Reanalysis Version 2c. Research Data Archive at the National Center for Atmospheric Research, Computational and Information Systems Laboratory. http://rda.ucar.edu/datasets/ds131.2/ (accessed 8 January 2016).

Cropper, T.E., E. Hanna, M.A. Valente, T. Jonsson (2015) A daily Azores–Iceland North Atlantic Oscillation index back to 1850. *Geoscience Data Journal* 2, 12-24.

Davini, P., C. Cagnazzo, S. Gualdi, A. Navarra (2012a) Bidimensional diagnostics, variability, and trends of northern hemisphere blocking. *J. Clim.* 25, 6496-6509.

Davini, P., C. Cagnazzo, R. Neale, J. Tribbia (2012b) Coupling between Greenland blocking and the North Atlantic Oscillation pattern. *Geophys. Res. Lett.* 39, L14701.

DeWeaver, E. and S. Nigam (2000) Do stationary waves drive the zonal-mean jet anomalies of the northern winter? *J. Clim.* 13, 2160-2176.

Ding, Q., J.M. Wallace, D.S. Battisti, E.J. Steig, A.J.E. Gallant, H.-J. Kim, L. Geng (2014) Tropical forcing of the recent rapid Arctic warming in northeastern Canada and Greenland. *Nature* 509, 209-213.

Ding, Q., A. Schweiger, M. L'Heureux, D.S. Battisti, S. Po-Chedley, N.C. Johnson, E. Blanchard-Wrigglesworth, K. Harnos, Q. Zhang, R. Eastman, E.J. Steig (2017) Influence of high-latitude atmospheric circulation changes on summertime Arctic sea ice. *Nat. Clim. Change* 7, 289-295.

Duchon, C.E. (1979) Lanczos filtering in one and two dimensions. *J. Appl. Meteorol.* 18, 1016-1022.

Fang, Z.-F. (2004) Statistical relationship between the northern hemisphere sea ice and atmospheric circulation during winter time. In *Observation, Theory and Modeling of Atmospheric Variability. World Scientific Serieson Meteorology of East Asia*, Zhu, X. (Ed.) World Scientific Publishing Company: Singapore, 131–141.

Fenty, I., and P. Heimbach (2013) Coupled sea ice-ocean-state estimation in the Labrador Sea and Baffin Bay. *J. Phys. Oceanog.* 43, 884-904.

Franzke, C., S. Lee, S.B. Feldstein (2004) Is the North Atlantic Oscillation a breaking wave? *J. Atmos. Sci.* 61, 145-160.

Hall, R.J. (2016) *The North Atlantic Polar Front Jet Stream: Variability and Predictability, 1871-2014.* PhD thesis, University of Sheffield.

Hall, R.J., E. Hanna. (2018) North Atlantic circulation indices: links with summer and winter UK temperatures and precipitation and implications for seasonal forecasting. *Int. J. Climatol.*, doi: 10.1002/joc.5398.

Hall, R., R. Erdelyi, E. Hanna, J.M. Jones, A.A. Scaife (2015) Drivers of North Atlantic Polar Front jet stream variability. *Int. J. Climatol.* 35. 1697-1720.

Hanna, E., P. Huybrechts. K. Steffen, J. Cappelen, R. Huff, C. Shuman. T. Irvine-Fynn, S. Wise, M. Griffiths (2008) Increased runoff from melt from the Greenland Ice Sheet: a response to global warming. *J. Clim.* 21, 331-341.

Hanna, E., J. Cappelen, X. Fettweis, P. Huybrechts, A. Luckman, M.H. Ribergaard (2009) Hydrologic response of the Greenland ice sheet: the role of oceanographic warming. *Hydrol. Proc.* 23, 7-30.

Hanna, E., S.H. Mernild, J. Cappelen, K. Steffen (2012) Recent warming in Greenland in a long-term instrumental (1881-2012) climatic context: I. Evaluation of surface air temperature records. *Environ. Res. Lett.* 7, 045404.

Hanna, E., J.M. Jones, J. Cappelen, S.H. Mernild, L. Wood, K. Steffen, P. Huybrechts (2013) The influence of North Atlantic atmospheric and oceanic forcing effects on 1900-2010 Greenland summer climate and ice melt/runoff. *Int. J. Climatol.* 33, 862-880.

Hanna, E., X. Fettweis, S.H. Mernild, J. Cappelen, M.H. Ribergaard, C.A. Shuman, K. Steffen, L. Wood, T.L. Mote (2014) Atmospheric and oceanic climate forcing of the exceptional Greenland ice sheet surface melt in summer 2012. *Int. J. Climatol.* 34, 1022-1037.

Hanna, E., T.E. Cropper, P.D. Jones, A.A. Scaife, R. Allan (2015) Recent seasonal asymmetric changes in the NAO (a marked summer decline and increased winter variability) and associated changes in the AO and Greenland Blocking Index. *Int. J. Climatol.* 35, 2540-2554.

Hanna, E., T.E. Cropper, R.J. Hall, J. Cappelen (2016) Greenland Blocking Index 1851-2015: a regional climate change signal. *Int. J. Climatol.* 36, 4847-4861.

Hanna, E., R.J. Hall, J.E. Overland (2017) Can Arctic warming influence UK extreme weather? *Weather* 72, 346-352.

Hofer, S., A.J. Tedstone, X. Fettweis, J.L. Bamber (2017) Decreasing cloud cover drives the recent mass loss on the Greenland ice sheet. *Science Advances* 3, e1700584.

Kalnay, E. et al. (1996) The NCEP/NCAR 40-year reanalysis project. *Bull. Amer. Meteor. Soc.* 77, 437-470.

Liu, C., E. A. Barnes (2015), Extreme moisture transport into the Arctic linked to Rossby wave breaking. *J. Geophys. Res. Atmos.* 120, 3774–3788.

Luo, D., T. Gong, Y. Diao (2007a) Dynamics of eddy-driven low-frequency dipole modes. Part III: meridional displacement of westerly jet anomalies during two phases of NAO. *J. Atmos. Sci.* 64, 3232-3248.

Luo, D., A.R. Lupo, H. Wan (2007b) Dynamics of eddy-driven low-frequency dipole modes. Part I: A simple model of North Atlantic Oscillations. *J. Atmos. Sci.* 64, 3-28.

Markus T., J.C. Stroeve, J. Miller (2009) Recent changes in Arctic sea ice melt onset, freezeup, and melt season length. *J. Geophys. Res.* 114:C12024, doi:10.1029/2009JC005436.

Mattingly, K. S., J.T. McLeod, J.A. Knox, J.M. Shepherd, T.L. Mote (2015) A climatological assessment of Greenland blocking conditions associated with the track of Hurricane Sandy and historical North Atlantic hurricanes. *Int. J. Climatol.* 35, 746–760.

McLeod, J., T. Mote (2015) Assessing the role of precursor cyclones on the formation of extreme Greenland blocking episodes and their impact on summer melting across the Greenland ice sheet. *J. Geophys. Res.* 120, 12357-12377.

McLeod, J.T., T.L. Mote (2016) Linking interannual variability in extreme Greenland blocking episodes to the recent increase in summer melting across the Greenland ice sheet. *Int. J. Climatol.* 36, 1484–1499.

Neff, W., G. P. Compo, F. M. Ralph, and M. D. Shupe (2014) Continental heat anomalies and the extreme melting of the Greenland ice surface in 2012 and 1889. *J. Geophys. Res.* 119, 6520–6536.

Orr, A., E. Hanna, J.C.R. Hunt, J. Cappelen, K. Steffen, A.G. Stephens (2005) Characteristics of stable flows over southern Greenland. *Pure and Applied Geophysics* 162, 1747-1778.

Overland, J.E., M. Wang (2015) Increased variability in early winter subarctic North American atmospheric circulation. *J. Clim.* 28, 7297–7305.

Overland, J. E., J.A. Francis, E. Hanna, M. Wang (2012) The recent shift in early summer Arctic atmospheric circulation. *Geophys. Res. Lett.* 39 (19).

Overland, J., J.A. Francis, R. Hall, E. Hanna, S.-J. Kim, T. Vihma (2015) The melting Arctic and midlatitude weather patterns: are they connected? *J. Clim.* 28, 7917-7932.

Overland, J.E., K. Dethloff, J.A. Francis, R.J. Hall, E. Hanna, S.-J. Kim, J.A. Screen, T.G. Shepherd, T. Vihma (2016) Nonlinear response of mid-latitude weather to the changing Arctic. *Nat. Clim. Change* 6, 992-999.

Park, H.-S., S. Lee, S.-W. Son, S.B. Feldstein, Y. Kosaka (2015) The impact of poleward moisture and sensible heat flux on Arctic winter sea ice variability. *J. Clim.* 28, 5030-5040.

Parker, D.E., T.P. Legg, C.K. Folland (1992) A new daily Central England Temperature series, 1772-1991. *Int. J. Climatol.* 12, 317-342.

Parry, S., T. Marsh, M. Kendon (2013) 2012: from drought to floods in England and Wales. *Weather* 68, 268–274.

Priestley, M. D. K., J. G. Pinto, H. F. Dacre, L. C. Shaffrey (2017) Rossby wave breaking, the upper level jet, and serial clustering of extratropical cyclones in western Europe. *Geophys. Res. Lett.* 44, 514–521.

Rayner, N. A., D. E. Parker, E. B. Horton, C. K. Folland, L. V. Alexander, D. P. Rowell, E. C. Kent, A. Kaplan (2003) Global analyses of sea surface temperature, sea ice, and night marine air temperature since the late nineteenth century. *J. Geophys. Res.* 108, 4407.

Rex, D.F. (1950) Blocking action in the middle troposphere and its effect upon regional climate. *Tellus* 2, 196-211.

Rimbu, N., G. Lohmann, M. Werner, M. Ionita (2017) Links between central Greenland stable isotopes, blocking and extreme climate variability over Europe at decadal to multidecadal time scales. *Clim. Dyn.* 49, 649-663.

Scorer, R.S. (1988) Sunny Greenland. *Q.J. Roy. Meteorol. Soc.* 114, 3-29.

Serreze, M., J. Stroeve (2015) Arctic sea ice trends, variability and implications for seasonal forecasting. *Philosophical Transactions of the Royal Society A* 373: 20140159.

Tedesco, M., T. Mote, X. Fettweis, E. Hanna, J. Jeyaratnam, J.F. Booth, R. Datta, K. Briggs (2016a) Arctic cut-off high drives the poleward shift of a new Greenland melting record. *Nat. Comm.* 7 (11723).

Tedesco, M., S. Doherty, X. Fettweis, P. Alexander, J. Jeyaratnam, J. Stroeve (2016b) The darkening of the Greenland ice sheet: trends, drivers, and projections (1981–2100). *The Cryosphere* 10, 477-496.

Titchner, H. A., N. A. Rayner (2014) The Met Office Hadley Centre sea ice and sea surface temperature data set, version 2: 1. Sea ice concentrations. *J. Geophys. Res. Atmos.* 119, 2864–2889.

Trenberth, K.E., J.T. Fasullo, G. Branstator, A.S. Phillips (2014) Seasonal aspects of the recent pause in surface warming. *Nat. Clim. Change* 4, 911-926.

van den Broeke, M. R., J. Box, X. Fettweis, E. Hanna, B. Noël, M. Tedesco, D. van As, W. J. van de Berg and L. van Kampenhout (2017) Greenland ice sheet surface mass loss: recent developments in observation and modelling. *Current Climate Change Reports*, doi.org/10.1007/s40641-017-0084-8.

Woollings, T., B. Hoskins, M. Blackburn, P. Berrisford (2008) A new Rossby wave-breaking interpretation of the North Atlantic Oscillation. *J. Clim.* 65, 609-626.

Woollings, T., A. Hannachi, B. Hoskins (2010) Variability of the North Atlantic eddy-driven jet stream. *Q.J. Roy. Meteorol. Soc.* 136, 856-868.

Yoo, C., S. Lee, S.B. Feldstein (2012) Mechanisms of Arctic surface air temperature change in response to the Madden-Julian Oscillation. *J. Clim.* 25, 5777-5790.

Table 1. Mean numbers of days per calendar month and season with **<u>GBI values > 1</u>** for specified decades and other periods. Highest values for each month and season are emboldened. Recent climatological values are highlighted in grey.

Month/ season	1981-2010	2006-2015	2000-2009	1990-1999	1980-1989	1970-1979	1960-1969	1950-1959	1940-1949	1930-1939	1920-1929	1910-1919	1900-1909	1851-1899
Jan	2.9	3.7	3.4	1.2	4.2	4.2	**8.5**	5.4	5.9	3.6	2.7	3.9	1.3	3.2
Feb	4.6	6.2	5.7	1.6	4.9	2.9	7.6	5.7	**7.8**	5.1	1.5	2.2	6.5	3.7
Mar	5.2	7.8	5.8	5.2	4.4	4.5	3.8	7.2	5.5	7.5	4.9	7.1	**7.6**	5.5
Apr	5.1	4.4	3.3	**7.5**	3.7	6.0	3.1	5.0	2.4	2.3	4.8	2.0	3.5	4.0
May	5.5	6.6	5.9	5.7	4.8	4.8	3.9	**6.9**	3.8	4.1	5.5	1.7	6.3	3.3
Jun	7.1	**11.2**	8.0	7.0	5.5	2.9	1.4	7.1	5.4	5.2	6.9	6.2	8.0	4.9
Jul	6.3	**12.7**	10.1	6.5	2.3	6.0	6.1	5.1	5.1	7.4	3.0	11.2	4.1	6.0
Aug	5.2	**11.7**	7.8	2.4	5.1	4.7	7.6	5.7	3.4	5.8	4.1	6.8	3.5	5.3
Sep	6.3	5.2	5.3	7.1	5.4	3.7	4.5	4.9	2.8	**9.7**	4.3	6.0	5.1	5.8
Oct	7.2	8.9	**9.7**	6.4	5.1	5.6	4.6	2.9	6.2	4.6	5.6	4.9	4.3	8.4
Nov	4.6	2.9	3.0	5.6	5.0	1.4	5.3	5.1	5.9	2.2	4.2	5.7	5.8	**6.5**
Dec	6.1	7.0	7.1	3.6	5.8	4.8	**7.2**	5.3	4.6	5.5	4.4	3.5	2.5	4.4
ANN	66.1	**85.3**	75.1	59.8	56.2	51.5	63.6	66.3	58.8	63.0	51.9	61.2	58.5	61.1
JJA	18.6	**35.6**	25.9	15.9	12.9	13.6	15.1	17.9	13.9	18.4	14.0	24.2	15.6	16.2
DJF	13.0	17.2	13.9	7.4	14.2	12.0	**23.2**	16.1	19.1	13.4	8.6	10.1	10.8	11.3

Table 2. Linear trends in Greenland Blocking Index standard deviation of daily values, highest and lowest daily values, and numbers of days with GBI>0,1,2 for several months/seasons and different time periods. Units are normalised GBI values and (last three categories) numbers of days. Significant trends (p≤0.05) are highlighted in bold.

Parameter	Month/season	1900-2015	1950-2015	1990-2015
GBI standard deviation of daily values	Jun	**-0.16**	0.00	-0.18
“	Jul	-0.14	**0.16**	-0.04
“	Dec	-0.01	0.07	-0.03
GBI highest daily value	Jun	-0.31	0.40	0.17
“	Jul	-0.17	0.44	**0.88**
“	Dec	0.17	0.55	0.12
GBI lowest daily value	Jun	0.35	0.23	**0.84**
“	Jul	**0.47**	0.11	**1.14**
“	Dec	0.31	0.15	0.33
No. of days with GBI>0	Jun	1.29	**7.35**	**10.81**
“	Jul	3.84	5.83	**14.25**
“	Dec	0.58	0.05	3.39
“	ANN	16.81	15.79	**65.62**
“	JJA	6.10	**15.74**	**38.84**
“	DJF	6.34	-3.32	**24.08**
No. of days with GBI>1	Jun	0.85	**6.37**	6.47
“	Jul	2.31	**5.98**	**8.76**
“	Dec	3.17	0.43	4.32
“	ANN	**14.42**	18.45	**43.11**
“	JJA	6.06	**15.23**	**28.50**
“	DJF	4.01	-4.46	13.37
No. of days with GBI>2	Jun	-0.37	1.27	1.90
“	Jul	-0.10	1.89	4.12
“	Dec	**1.59**	1.25	1.01
“	ANN	5.82	7.92	**19.62**
“	JJA	1.93	**5.58**	11.16
“	DJF	1.03	-0.09	4.76

Table 3(a). Rank-ordered **summers (JJA)** with the most number (nd) of GBI>1 days, with corresponding numbers of days in those seasons reaching different GBI and NAO thresholds, and means and standard deviations of daily GBI and NAO values.

Year (JJA)	*nd GBI>1*	*nd GBI>0*	*nd GBI>2*	*nd NAO <-1*	*nd NAO <0*	*nd NAO <-2*	*GBI mean*	*GBI stdev*	*NAO mean*	*NAO stdev*
2012	57	79	15	34	64	12	2.11	0.93	-0.59	1.39
2008	47	67	16	20	39	7	1.42	1.23	0.36	1.68
1887	44	77	11	30	53	16	1.64	0.89	-0.39	1.49
2011	44	83	16	15	52	1	1.58	0.84	-0.07	1.02
1895	39	64	13	29	58	18	1.17	1.14	-0.36	1.75
1877	38	67	13	33	50	20	1.20	1.17	-0.43	2.12
1911	38	66	7	41	55	26	1.21	1.06	-0.63	1.77
1912	38	69	5	27	57	12	0.97	1.04	-0.43	1.29
1931	38	66	15	30	45	14	1.41	1.07	-0.26	1.78
2007	38	80	8	26	45	16	1.55	0.76	-0.20	1.57
1891	37	65	14	38	63	23	1.23	1.13	-0.78	1.61
1893	37	84	13	40	65	28	1.71	0.83	-0.97	1.71
2009	37	74	11	31	50	16	1.43	0.96	-0.40	1.83

Table 3(b). Rank-ordered **<u>winters (DJF)</u>** with the most number (nd) of GBI>1 days, with corresponding numbers of days in those seasons reaching different GBI and NAO thresholds, and means and standard deviations of daily GBI and NAO values.

Year (DJF)	*nd GBI>1*	*nd GBI>0*	*nd GBI>2*	*nd NAO <-1*	*nd NAO <0*	*nd NAO <-2*	*GBI mean*	*GBI stdev*	*NAO mean*	*NAO stdev*
2010	59	79	25	63	76	43	2.12	0.99	-1.87	1.70
1969	42	73	13	63	75	30	1.57	0.88	-1.43	1.28
1960	37	56	12	38	57	24	0.99	1.11	-0.63	1.77
2011	37	57	19	46	61	31	1.20	1.49	-0.91	1.95
1879	36	61	16	41	60	28	1.28	1.19	-0.86	1.69
1881	36	69	2	58	71	33	1.06	0.91	-1.60	1.77
1936	36	76	0	57	73	22	1.26	0.64	-1.14	1.31
1855	34	66	3	49	72	31	0.88	0.88	-1.30	1.48
1941	34	59	5	42	63	20	0.91	1.04	-0.71	1.63
1940	33	69	11	42	72	21	1.20	0.99	-1.01	1.27
1947	32	50	13	36	56	14	0.72	1.24	-0.46	1.75
1895	31	64	6	45	61	26	1.02	0.92	-1.13	2.06
1901	31	41	17	35	56	18	0.50	1.33	-0.44	1.64

Table 4. De-trended correlation coefficients between numbers of days/month above or below stated GBI thresholds and (a) monthly mean GBI, (b) monthly mean NAO, and (c) numbers of days/month above and below NAO threshold of opposite sign and value. Finally (d) compares numbers of moderate and extreme NAO days with monthly mean GBI values. All the above are based on 1851-2015 data (see main text, Section 2, for dataset details). All values above 0.2 or below -0.2 are statistically significant (p<0.01); red type denotes insignificant values.

(a)	Month	GBI>2	GBI>1	GBI>0	GBI<-1	GBI<-2
GBI	Jan	0.63	0.86	0.92	-0.72	-0.28
“	Feb	0.65	0.88	0.94	-0.81	-0.23
“	Mar	0.62	0.87	0.93	-0.74	-0.50
“	Apr	0.40	0.75	0.91	-0.87	-0.53
“	May	0.77	0.77	0.90	-0.78	-0.47
“	Jun	0.65	0.85	0.93	-0.76	-0.34
“	Jul	0.63	0.87	0.92	-0.77	-0.53
“	Aug	0.67	0.85	0.92	-0.73	-0.47
“	Sep	0.62	0.85	0.92	-0.74	-0.37
“	Oct	0.68	0.90	0.90	-0.71	-0.40
“	Nov	0.60	0.85	0.91	-0.74	-0.43
“	Dec	0.66	0.89	0.92	-0.73	-0.21
“	ANN	0.72	0.88	0.90	-0.77	-0.48
“	JJA	0.71	0.87	0.93	-0.78	-0.43
“	DJF	0.67	0.90	0.92	-0.79	-0.34
(b)	Month	GBI>2	GBI>1	GBI>0	GBI<-1	GBI<-2
NAO	Jan	-0.53	-0.77	-0.74	0.44	0.16
“	Feb	-0.58	-0.78	-0.81	0.66	0.14
“	Mar	-0.52	-0.71	-0.75	0.59	0.36
“	Apr	-0.23	-0.48	-0.66	0.54	0.30
“	May	-0.52	-0.52	-0.65	0.53	0.34
“	Jun	-0.45	-0.59	-0.67	0.51	0.27
“	Jul	-0.33	-0.45	-0.29	0.20	0.15
“	Aug	-0.41	-0.52	-0.46	0.12	0.05
“	Sep	-0.43	-0.54	-0.57	0.34	0.19
“	Oct	-0.51	-0.63	-0.63	0.49	0.22
“	Nov	-0.40	-0.66	-0.73	0.53	0.23
“	Dec	-0.66	-0.74	-0.70	0.49	0.12
“	JJA	-0.33	-0.44	-0.38	0.13	0.06

“	DJF	-0.65	-0.81	-0.75	0.54	0.21
(c)	Month	GBI>2	GBI>1	GBI>0	GBI<-1	GBI<-2
Ndays NAO<-2,-1,0;>1,2.	Jan	0.52	0.77	0.75	0.52	0.26
“	Feb	0.64	0.80	0.82	0.70	0.20
“	Mar	0.56	0.73	0.77	0.63	0.42
“	Apr	0.16	0.48	0.66	0.55	0.30
“	May	0.43	0.43	0.61	0.59	0.39
“	Jun	0.49	0.59	0.69	0.54	0.32
“	Jul	0.29	0.43	0.34	0.23	0.22
“	Aug	0.42	0.49	0.47	0.11	0.00
“	Sep	0.38	0.54	0.58	0.32	0.25
“	Oct	0.52	0.62	0.63	0.52	0.26
“	Nov	0.39	0.67	0.74	0.58	0.28
“	Dec	0.76	0.74	0.70	0.55	0.14
“	ANN	0.51	0.57	0.64	0.45	0.23
“	JJA	0.40	0.44	0.44	0.20	0.09
“	DJF	0.71	0.80	0.77	0.61	0.27

(d)	Month	NAO<-2	NAO<-1	NAO<0	NAO>1	NAO>2
GBI	Jan	0.70	0.76	0.79	-0.75	-0.59
“	Feb	0.72	0.80	0.84	-0.78	-0.66
“	Mar	0.64	0.75	0.79	-0.75	-0.65
“	Apr	0.42	0.54	0.61	-0.61	-0.52
“	May	0.54	0.54	0.62	-0.65	-0.59
“	Jun	0.50	0.63	0.66	-0.66	-0.52
“	Jul	0.24	0.34	0.39	-0.36	-0.31
“	Aug	0.45	0.44	0.45	-0.40	-0.25
“	Sep	0.48	0.56	0.57	-0.50	-0.38
“	Oct	0.62	0.63	0.65	-0.63	-0.50
“	Nov	0.57	0.70	0.73	-0.71	-0.54
“	Dec	0.68	0.72	0.74	-0.67	-0.61
“	ANN	0.49	0.50	0.49	-0.48	-0.39
“	JJA	0.34	0.37	0.39	-0.37	-0.23
“	DJF	0.72	0.78	0.79	-0.76	-0.66

Table 5(a). Anomalously high GBI events (≥3σ for ≥3 consecutive days), with concomitant NAO values, in reverse chronological order. Lag between GBI peak and NAO trough, and mean and extreme CET/EWP values during these dates, are also given; *extreme values are within ±5 days of the respective peak GBI dates. Several closely-spaced recent events that occurred during consecutive Octobers between 2002 and 2006 are highlighted in green. Mean CET anomalies (EWP values) <-1σ (>2 mm) are highlighted in blue; mean CET anomalies >+1σ are highlighted in yellow.

Dates	Mean GBI value for period	Highest GBI value in period	Mean C15 NAO value	Lowest C15 NAO value in period	C15 (CPC) NAO lag wrt GBI	Mean CET anomaly (σ)	Greatest CET anomaly (σ)	Mean daily EWP (mm)	Max daily EWP (mm)
2010 Dec 15-21	3.78	5.10	-3.48	-4.19	0&5 (2)	-2.26	-3.53	1.39	3.74
2010 Nov 25-27	3.45	3.61	-3.50	-3.57	1 (0&4)	-2.20	*-3.13	1.14	*3.40
2010 Aug 19-21	3.31	3.50	-1.36	-1.75	0 (0)	0.56	1.23	4.34	*21.33
2010 Jan 2-4	3.19	3.34	-3.86	-5.05	0 (0)	-1.49	-2.27	1.00	*4.06
2009 Jul 16-18	3.12	3.17	0.69	0.05	4 (-2)	-0.28	*-0.79	11.32	20.09
2006 Oct 16-20	3.63	4.29	-2.73	-3.73	-1 (3)	1.55	*2.03	4.99	*12.90
2006 May 9-11	3.07	3.12	-2.75	-3.08	3 (0)	1.49	1.73	0.42	*8.36
2005 Oct 18-21	3.38	3.54	-1.53	-2.01	-2 (2)	0.71	*1.85	7.14	*20.37
2003 Oct 17-20	3.54	3.84	-2.50	-3.17	0 (2)	-0.58	*-2.81	0.32	*5.20
2002 Oct 16-21	3.42	3.91	-4.02	-7.24	1 (3)	-1.28	-2.21	6.24	*21.52
1997 Nov 30-Dec 2	3.21	3.38	-2.04	-2.28	0 (-1)	-0.54	*-1.54	3.33	9.96
1995 Apr 25-27	3.20	3.40	-3.52	-4.07	0 (-1)	0.32	2.16	0.33	*8.59

1964 Aug 13-15	3.40	3.57	-3.46	-3.96	-1 (0)	-0.18	*-2.14	1.57	*10.45
1944 Jul 22-25	3.34	3.76	-3.80	-4.38	1	-0.38	*-1.17	0.60	*3.87
1929 Jan 26-28	4.06	4.49	-4.09	-4.42	0	-1.30	-1.63	N/A	N/A
1919 Jul 21-23	3.63	3.89	-0.74	-1.51	3	-1.05	*-2.00	N/A	N/A
1918 Jul 20-22	3.64	3.84	-1.51	-2.08	-5	-0.19	-1.26	N/A	N/A
1916 Sep 28-Oct 1	3.22	3.40	-3.10	-3.80	0	-0.00	*1.77	N/A	N/A
1902 Jul 22-24	3.44	3.56	-3.75	-4.38	0	-1.52	*-2.57	N/A	N/A
1900 Mar 24-26	3.39	3.73	-2.62	-3.25	0	-1.89	-2.05	N/A	N/A
1899 Dec 28-31	3.26	3.38	-2.55	-3.16	-1	-0.14	*-2.04	N/A	N/A
1897 Jun 5-7	3.19	3.28	-2.97	-3.19	-1	1.09	*1.96	N/A	N/A
1895 Oct 20-23	3.42	3.82	-5.16	-5.76	1	-1.75	*-3.59	N/A	N/A
1894 May 18-20	3.65	3.93	-2.34	-2.65	0	-1.23	*-2.80	N/A	N/A
1888 Sep 29-Oct 3	3.57	4.27	-3.83	-5.14	0	-2.19	-4.00	N/A	N/A
1880 Oct 18-22	3.44	3.62	-4.47	-5.40	0	-2.27	-3.23	N/A	N/A
1880 Sep 30-Oct 4	3.69	3.88	-4.90	-6.64	1	-0.94	-2.80	N/A	N/A
1878 Dec 10-14	3.30	3.63	-2.89	-3.44	-1 & +6	-2.56	-3.27	N/A	N/A
1878 Nov 3-8	3.74	4.14	-2.48	-3.11	-8	-1.85	*-1.95	N/A	N/A
1876 Aug 22-24	3.32	3.55	-0.36	-0.81	0	1.13	*3.32	N/A	N/A
1875 Jul 22-24	3.48	3.79	-3.97	-4.67	-1	-0.44	*-1.41	N/A	N/A
1851 Nov 30-Dec 2	3.18	3.41	-1.99	-2.35	-4	-1.26	*-1.81	N/A	N/A

Table 5(b). Anomalously low GBI events (generally <-2.5σ for ≥3 consecutive days but <-2.0σ for ≥3 consecutive days for 1990-2015), with concomitant NAO values, in reverse chronological order. Extreme value nomenclature and colour coding are as for Table 5(a).

Dates	Mean GBI value for period	Lowest GBI value in period	Mean C15 NAO value	Highest C15 NAO value in period	C15 (CPC) NAO lag wrt GBI	Mean CET anomaly (σ)	Greatest CET anomaly (σ)	Mean daily EWP (mm)	Max daily EWP (mm)
2013 Apr 19-22	-2.19	-2.42	1.87	3.36	3 (3)	-0.33	*1.86	0.38	*3.15
2011 Apr 19-21	-2.25	-2.43	1.25	1.80	4 (-5,0,5)	2.17	*3.22	0.01	*0.94

2011 Apr 11-17	-2.31	-2.54	1.16	3.12	-3 (1)	0.81	*3.27	0.25	*0.89
2011 Apr 14-16	-2.52	-2.54	0.81	1.75	-3 (1)	1.08	*2.59	0.04	*0.89
2011 Apr 4-7	-2.44	-2.85	0.79	1.81	0? (1-2)	1.97	3.27	1.05	*6.54
1999 Aug 31-Sep 2	-2.65	-2.74	2.09	2.20	3 (1)	1.14	*2.21	0.04	*3.85
1993 Nov 9-13	-2.24	-2.45	2.55	3.79	-2 (-1)	-0.25	*-1.34	9.42	21.04
1993 Mar 14-18	-2.20	-2.49	0.93	2.58	0 (1)	1.52	1.86	0.43	*6.76
1991 Aug 25-27	-2.51	-2.81	0.96	1.51	0 (1 & -2)	0.85	*1.85	0.18	*5.27
1991 Aug 18-21	-2.05	-2.09	1.15	1.42	? (0)	0.14	*1.34	0.27	*5.27
1990 Apr 11-15	-2.43	-2.71	4.37	5.15	1 (0)	0.13	1.35	2.28	3.83
1990 Apr 12-14	-2.63	-2.71	4.10	5.15	1 (0)	0.10	1.35	3.33	3.83
1955 Sep 4-6	-2.86	-3.04	2.68	3.56	-1 (0)	0.60	*2.00	2.67	4.79
1935 Jul 10-13	-2.96	-3.05	2.49	3.25	-1 & 4	1.66	2.34	0.39	*4.31
1934 Apr 30-May 3	-2.97	-3.32	3.69	4.10	-1	0.61	*-0.88	0.24	*10.55
1929 Jul 11-13	-2.74	-2.98	0.49	0.86	-1	0.30	*2.23	N/A	N/A
1920 Jul 27-29	-2.82	-2.93	2.84	3.62	1	-2.02	*2.64	N/A	N/A
1906 Apr 4-6	-2.94	-3.13	3.19	3.67	0	0.76	*-1.34	N/A	N/A
1897 Apr 13-15	-2.81	-2.93	4.06	4.97	0	0.37	1.10	N/A	N/A
1896 Nov 19-22	-2.63	-2.83	2.38	3.87	-2	-0.20	*-0.93	N/A	N/A
1876 Jun 1-3	-2.69	-2.75	2.86	3.40	3	0.13	*0.91	N/A	N/A
1855 Jul 21-23	-2.92	-3.20	1.00	3.05	0	0.50	1.84	N/A	N/A
1853 Aug 9-11	-2.62	-2.81	-1.55	-0.12	-2	-0.46	-1.61	N/A	N/A

Figure captions

Figure 1. Cumulative sum of daily GBI 1851-2015 time series for: (a) annual; and seasonal months in (b) winter, (c) spring, (d) summer and (e) autumn.

Figure 2. Annual, summer (JJA) and winter (DJF) seasonal series of GBI days per year of given thresholds (>0, >1, >2), 1851-2015. Linear trendlines are fitted through the annual data.

Figure 3. Running de-trended correlation coefficients between daily GBI and NAO values, showing variations in mean daily correlations over the seasonal cycle (correlation calculated for 1 January for all years, then repeated for each day of year) based on Cropper et al. (2015) Azores-Iceland station NAO series and (a) 1851-2015 and (b) 1950-2015 data. Panel (b) also includes GBI correlations with the 1950-2015 CPC NAO index (dotted blue line). In panel (c), correlations between GBI and station-based NAO are calculated for 1851 for all days, then repeated for all years. In all cases, a 7-point Gaussian filter has been applied to the raw correlation values for each day/year. Horizontal dashed lines show the $p \leq 0.05$ significance level for correlation coefficients.

Figure 4. Composite (mean) plots of anomalies of (a,b) 500 hPa geopotential height, (c,d) wind speed, (e,f) 850 hPa temperature, (g,h) sea-ice concentration, and (i,j) sea-

surface temperature for the five seasons/years with the highest numbers of GBI>1 days during 1851-2015. Plots a,c,e,g,i are for winter and b,d,f,h,j are for summer.

Figure 5. North Atlantic atmospheric circulation parameters during composite life cycles of various GBI episodes: (a) four (2002, 2003, 2005 and 2006) October *high* GBI episodes; (b) five (2 x 1880, 1888, 1895 & 1916) September/October *high* GBI episodes; (c) three (1964, 2009 & 2010) July/August *high* GBI episodes; (d) three (1997 & 2 x 2010) NDJ *high* GBI episodes; (e) seven (1897, 1906, 1934, 1990, 1993, 2011 & 2013) MAM *low* GBI episodes. See Table 5 for definitions of high and low thresholds (in caption) and for further details of these events.

Figure 6. Running de-trended correlation coefficients of daily (a,b) CET and (c,d) EWP with daily GBI and NAO values for 1851-2015 (CET) and 1931-2015 (EWP), including (a,c) variations in mean daily correlations over the seasonal cycle (correlation calculated for 1 January for all years, then repeated for each day of year) and (b,d) correlation calculated for 1851 (CET) and 1931 (EWP) for all days, then repeated for all years. A 7-point Gaussian filter has been applied to the raw correlation values for each day/year. Horizontal dashed lines show the $p \leq 0.05$ significance level for correlation coefficients.

Figure 1. Cumulative sum of daily GBI 1851-2015 time series for: (a) annual; and seasonal months in (b) winter, (c) spring, (d) summer and (e) autumn.

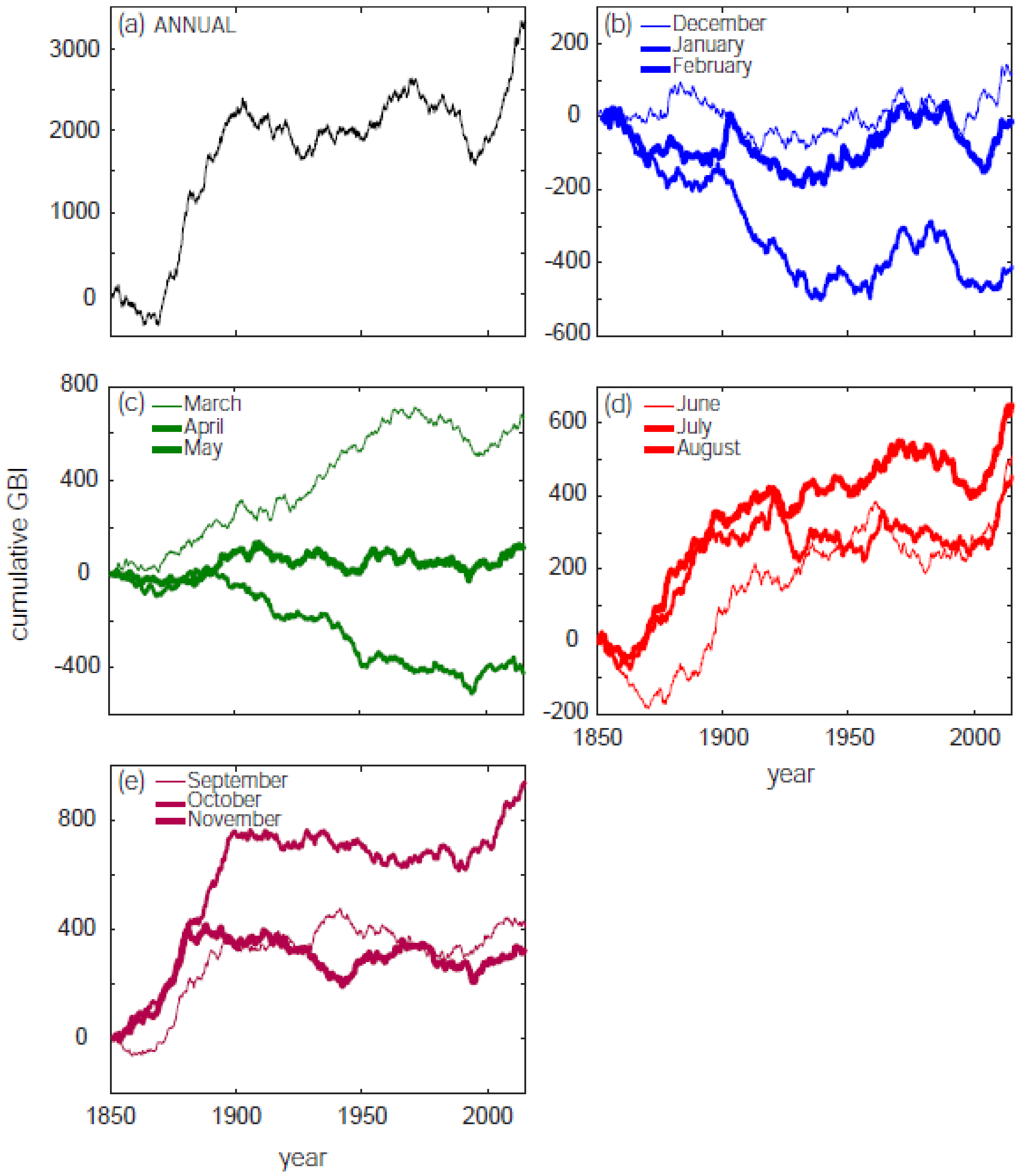

Figure 2. Annual, summer (JJA) and winter (DJF) seasonal series of GBI days per year of given thresholds (>0, >1, >2), 1851-2015. Linear trendlines are fitted through the annual data.

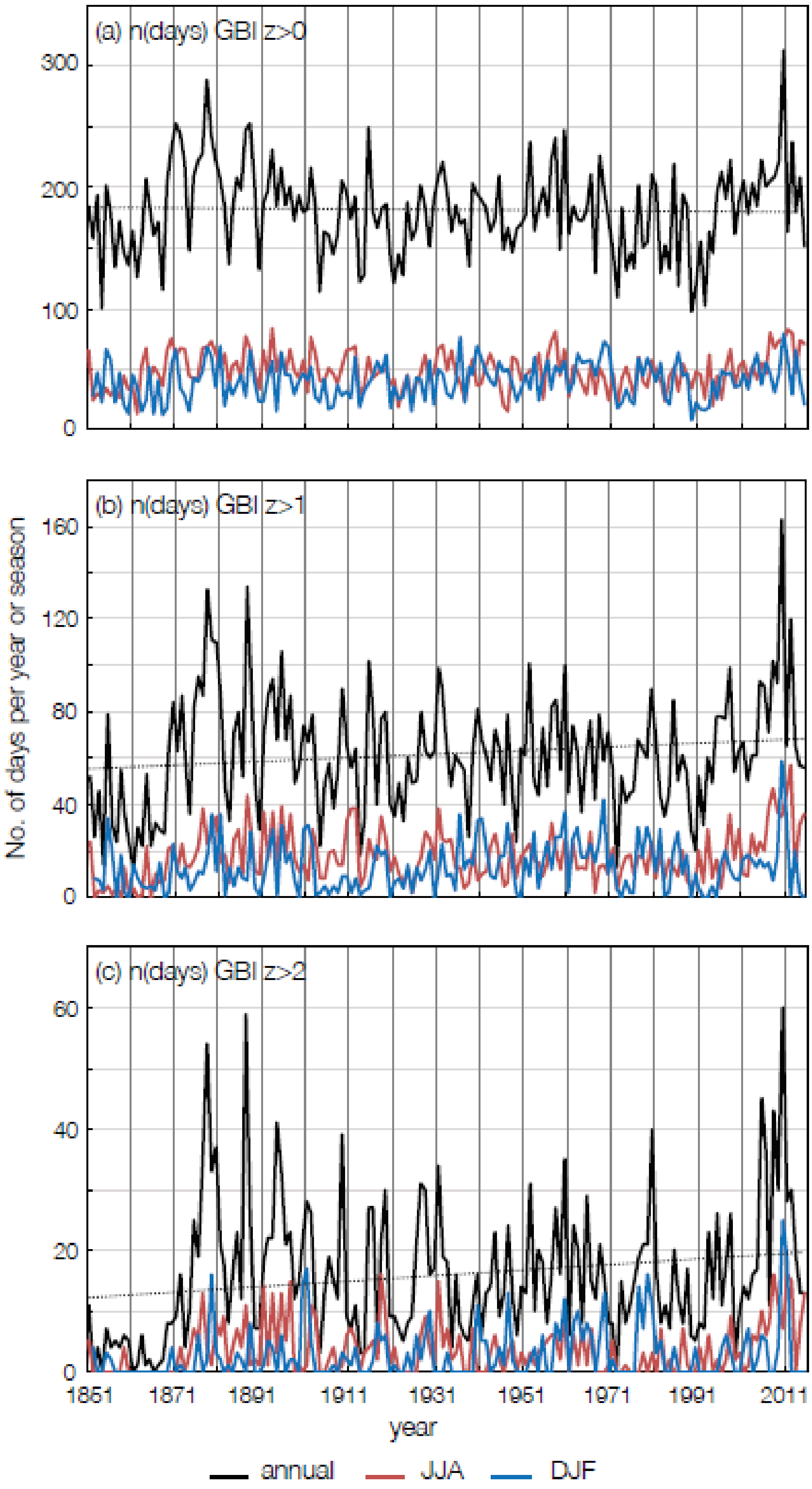

Figure 3. Running de-trended correlation coefficients between daily GBI and NAO values, showing variations in mean daily correlations over the seasonal cycle (correlation calculated for 1 January for all years, then repeated for each day of year) based on Cropper et al. (2015) Azores-Iceland station NAO series and (a) 1851-2015 and (b) 1950-2015 data. Panel (b) also includes GBI correlations with the 1950-2015 CPC NAO index (dotted blue line). In panel (c), correlations between GBI and station-based NAO are calculated for 1851 for all days, then repeated for all years. In all cases, a 7-point Gaussian filter has been applied to the raw correlation values for each day/year. Horizontal dashed lines show the p≤0.05 significance level for correlation coefficients.

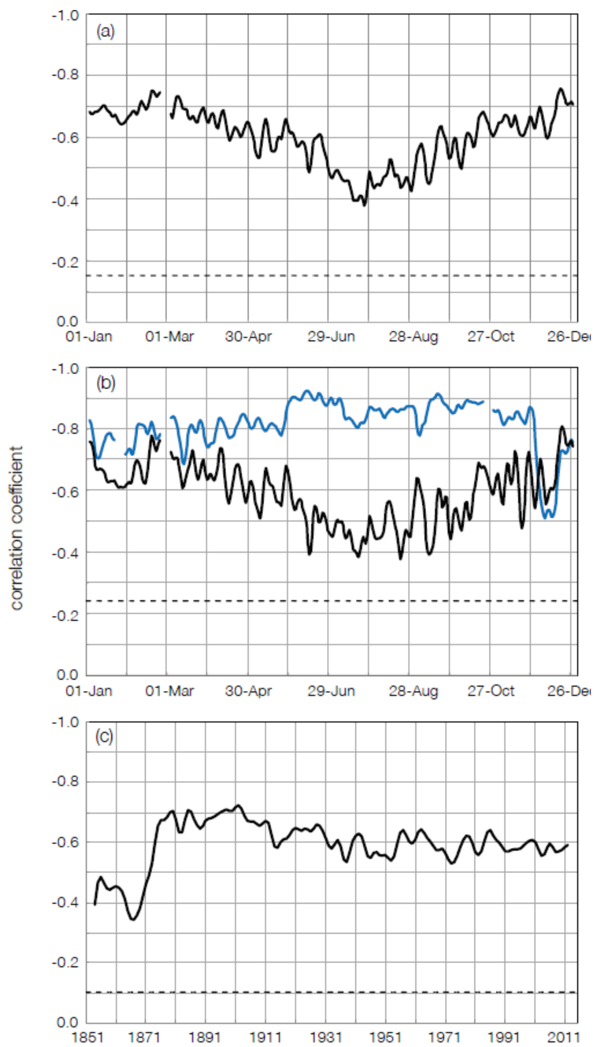

Figure 4. Composite (mean) plots of anomalies of (a,b) 500 hPa geopotential height, (c,d) wind speed, (e,f) 850 hPa temperature, (g,h) sea-ice concentration, and (i,j) sea-surface temperature for the five seasons/years with the highest numbers of GBI>1 days during 1851-2015. Plots a,c,e,g,i are for winter and b,d,f,h,j are for summer.

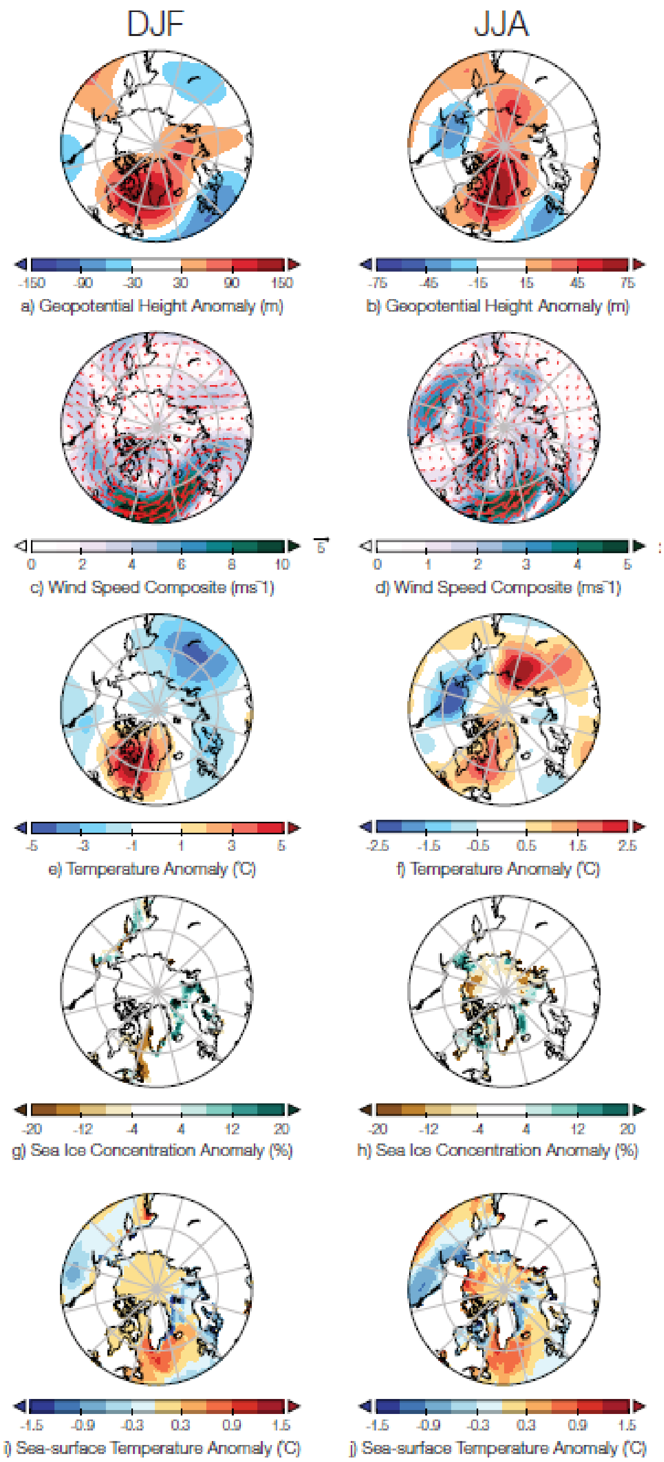

Figure 5. North Atlantic atmospheric circulation parameters during composite life cycles of various GBI episodes: (a) four (2002, 2003, 2005 and 2006) October *high* GBI episodes; (b) five (2 x 1880, 1888, 1895 & 1916) September/October *high* GBI episodes; (c) three (1964, 2009 & 2010) July/August *high* GBI episodes; (d) three (1997 & 2 x 2010) NDJ *high* GBI episodes; (e) seven (1897, 1906, 1934, 1990, 1993, 2011 & 2013) MAM *low* GBI episodes. See Table 5 for definitions of high and low thresholds (in caption) and for further details of these events.

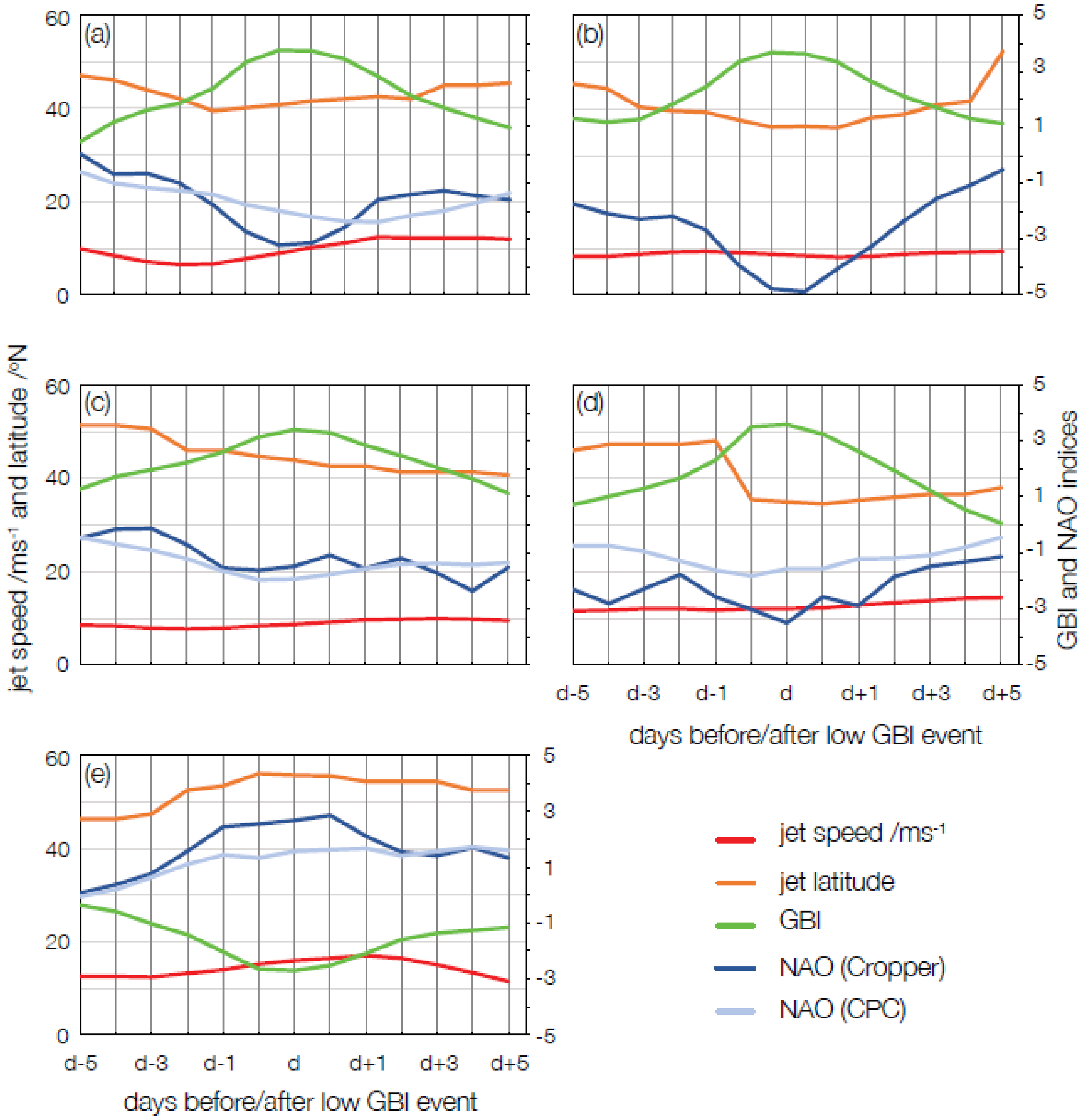

Figure 6. Running de-trended correlation coefficients of daily (a,b) CET and (c,d) EWP with daily GBI and NAO values for 1851-2015 (CET) and 1931-2015 (EWP), including (a,c) variations in mean daily correlations over the seasonal cycle (correlation calculated for 1 January for all years, then repeated for each day of year) and (b,d) correlation calculated for 1851 (CET) and 1931 (EWP) for all days, then repeated for all years. A 7-point Gaussian filter has been applied to the raw correlation values for each day/year. Horizontal dashed lines show the p≤0.05 significance level for correlation coefficients.